Available online at www.sciencedirect.com
ScienceDirect
Journal of Sound and Vibration 304 (2007) 811–830
JOURNAL OF SOUND AND VIBRATION
www.elsevier.com/locate/jsvi

# Free vibration analysis of circular plates with multiple circular holes using indirect BIEMs

W.M. Lee[a], J.T. Chen[b,*], Y.T. Lee[b]

[a]*Department of Mechanical Engineering, China Institute of Technology, Taipei, Taiwan*
[b]*Department of Harbor and River Engineering, National Taiwan Ocean University, Keelung, Taiwan*

Received 25 January 2007; accepted 18 March 2007
Available online 4 May 2007

**Abstract**

In this paper, a semi-analytical approach is proposed to solve natural frequencies and natural modes for circular plates with multiple circular holes by using the indirect formulation in conjunction with degenerate kernels and Fourier series. All the kernels in the indirect formulation are expanded into degenerate form. By uniformly collocating points on the boundary, a linear algebraic system can be constructed. The direct searching approach is adopted to determine the natural frequency through singular value decomposition (SVD). After determining the unknown Fourier coefficients, the corresponding mode shape is obtained by using the indirect boundary integral formulations. The results of the annular plate, as a special case, are compared with the analytical solution to verify the validity of the present method. For the cases of circular plates with multiple circular holes, the results are also compared with those of finite element method (FEM) using ABAQUS. Besides, the effect of eccentricity of the hole on the natural frequencies is also considered. Good accuracy, high rate of convergence and computational efficiency are the main features of the present method due to the semi-analytical procedure.


## 1. Introduction

Circular plates with multiple circular holes are widely used in engineering structures [1], e.g. missiles, aircraft, etc., either to reduce the weight of the whole structure or to increase the range of inspection. These holes in the structure usually cause the change of natural frequency as well as the decrease of the corresponding strength. The comprehension of the associated effects is helpful to the work of mechanical design and flight control of the structure. As quoted by Leissa [2]: "the free vibrations of circular plates have been of practical and academic interest for at least a century and a half", we revisit this problem by using a semi-analytical approach. Although the results for circular or annular plates are available in the literature [1–8]; however, few studies except [1] have done on the problem of plate with an eccentric hole. On the other hand, a large amount of papers on the circular membrane vibration with an eccentric hole have been published [9,10]. Recently some results on the problem of plate with an eccentric hole [11,12] or multiple holes [13] have

*Corresponding author. Tel.: +886 2 24622192x6177; fax: +886 2 24632375.
*E-mail address:* jtchen@mail.ntou.edu.tw (J.T. Chen).

0022-460X/$ - see front matter © 2007 Elsevier Ltd. All rights reserved.
doi:10.1016/j.jsv.2007.03.026

been reported. A study of the effect of the eccentricity on the free vibration of annular-like plates was previously conducted using the FEM [1,11]. In this case, more than 1500 elements [11] were required to achieve accurate solutions for the lower order vibration modes. The Rayleigh–Ritz variational method was also applied to the free vibration of circular plate with an eccentric hole [12].

In the past, some analytical solutions [3] for natural frequencies of the circular or annular plates were solved. Frequency equations are obtained by substituting the general solution, satisfied the governing equation of plates, into the boundary conditions. These results were confirmed experimentally but some analytic solutions corresponding to the clamped boundary condition showed an obvious deviation from the experimental results due to the lack of stiffness of the clamped boundary condition in reality. Since an analytical solution of natural frequencies requires the solution of special functions (e.g. Bessel function and modified Bessel function), Vera et al. [4–6] obtained analytical solutions by implementing the same procedure as [3] in the Maple V system and pointed out some inaccurate results in Ref. [14]. Regarding to the circular plate with multiple holes, the analytical solution of the natural frequencies and the corresponding mode shapes have not so far been solved due to the fourth-order partial differential equation and complex geometry configurations. To propose a semi-analytical approach for solving the circular plate with circular holes is not trivial and is the main goal of this research.

On the other hand, diverse numerical methods were resorted to the solution of plate problems, which include finite difference method (FDM), finite element method (FEM) and boundary element method (BEM). BEM has some advantages in comparison with domain discretization methods (FEM, FDM). The main gain is that the BEM reduces the dimension of the original problem by one, thus, the number of the introduced unknowns is much less than that of the traditional domain type methods. In addition, the domain mesh generation is not required, which is generally the most difficult and time consuming task. For the BEM applications to plate problems, readers may consult with the review article [15]. It is noted that improper integrals on the boundary should be handled particularly when the BEM is used. In the past, many researchers proposed several regularization techniques to deal with the singularity and hypersingularity. The determination of the Cauchy principal value (CPV) and the Hadamard principal value (HPV) in the singular and hypersingular integrals are critical issues in BEM/BIEM [16,17]. For the plate problem, it is more difficult to calculate the principle values since the kernels are involved with transcendental complex functions. Based on direct boundary integral formulation, Chen et al. [13,18,19] recently proposed null-field integral equations in conjunction with degenerate kernels and Fourier series to solve boundary value problems with circular boundaries. Some applications were done in the static stress calculations of anti-plane and plate problems. For the indirect BEM, Ventsel [20] has solved the static plate problems. In this paper, we utilize degenerate kernels and Fourier series to solve the plate eigenproblem. The expressions for the degenerate kernel can be derived by expanding the fundamental solution into a series form on each side of the boundary of the domain by employing the addition theorem. The introduction of degenerate kernel in companion with Fourier series can yield the exponential convergence [21,22] instead of the linear algebraic convergence in BEM. In reality, addition theorems are expansion formulae for the special functions (e.g. Bessel function, Legendre functions, spherical harmonics, etc.) in a selected coordinate system [23]. Therefore, degenerate kernel, namely separable kernel and Fourier series, are vital tools to study the circular plate with circular holes.

The purpose of this paper is to propose a semi-analytical approach to solve the natural frequencies and natural modes of circular plate with multiple circular holes by using the indirect boundary integral formulation in conjunction with degenerate kernels and Fourier series. The indirect formulation by choosing the single- and double-layer potential is proposed and the fictitious density distribution on the boundary is represented by using Fourier series in the adaptive coordinate system. A linear algebraic system is constructed by uniformly locating the collocation points on the boundary. By matching the boundary conditions, the determinant of the matrix must be zero to obtain the non-trivial eigensolution. The direct searching approach [24] is adopted to determine the natural frequency by using singular value decomposition (SVD). After determining the Fourier coefficients, the corresponding mode shape of the circular plate with multiple circular holes can be obtained by using the indirect boundary integral equations. For the plate problem, the slope (bending angle), moment and effective shear force in the normal and tangential directions for the non-concentric domain must be determined with care under the adaptive observer system. Therefore, the technique of vector and tensor transformation is adopted to deal with the problem for the non-concentric plate. Finally,

the analysis result of the annular plate, as our special case, is compared with the analytical solution [3–5,14] to verify the validity of the present method. The results of the circular plate with eccentric circular hole and multiple circular holes are compared with those of Khurasia [1], Cheng [11], Laura [12] and FEM using ABAQUS to demonstrate the generality of the proposed method.

## 2. Problem statement and indirect boundary integral formulation

### 2.1. Problem statement of plate eigenproblem

The governing equation for the free flexural vibration of a uniform thin plate with randomly distributed circular holes as shown in Fig. 1 is written as follows:

$$\nabla^4 u(x) = \lambda^4 u(x), \quad x \in \Omega, \tag{1}$$

where $u$ is the lateral displacement, $\lambda^4 = \omega^2 \rho_0 h/D$, $\lambda$ the dimensionless frequency parameter, $\omega$ the circular frequency, $\rho_0$ the volume density, $D$ the flexural rigidity expressed as $D = Eh^3/12(1-\nu^2)$ in terms of the Young's modulus $E$, the Poisson ratio $\nu$ and the plate thickness $h$, and $\Omega$ the domain of the thin plate.

### 2.2. Indirect boundary integral formulation

The kernel function $U(s, x)$ is the fundamental solution which satisfies

$$\nabla^4 U(s,x) - \lambda^4 U(s,x) = \delta(s-x), \tag{2}$$

where $\nabla^4$ is the biharmonic operator, $\delta(s-x)$ is the Dirac-delta function, and $s$ and $x$ are the source and field points, respectively. Considering the two singular solutions ($Y_0(\lambda r)$ and $K_0(\lambda r)$, which are the zeroth order of the second-kind Bessel and modified Bessel functions, respectively) [25] and two regular solutions ($J_0(\lambda r)$ and $I_0(\lambda r)$, which are the zeroth order of the first-kind Bessel and modified Bessel functions, respectively) in the fundamental solution, we have

$$U(s,x) = \frac{1}{8\lambda^2}\left[Y_0(\lambda r) + \mathrm{i}J_0(\lambda r) + \frac{2}{\pi}(K_0(\lambda r) + \mathrm{i}I_0(\lambda r))\right], \tag{3}$$

where $\mathrm{i}^2 = -1$ and $r \equiv |s-x|$ denotes the distance between the field point $x(\rho, \phi)$ and source point $s(R,\theta)$ in the polar coordinate. Based on the indirect boundary integral formulation, the displacement field of plate vibration can be represented by [9]

$$u(x) = \int_B P(s,x)\phi(s)\,\mathrm{d}B(s) + \int_B Q(s,x)\psi(s)\,\mathrm{d}B(s), \tag{4}$$

where $P(s, x)$ and $Q(s, x)$ are any two of the four kernel functions ($U$, $\Theta$, $M$ and $V$), which will be elaborated on later; $\phi(s)$ and $\psi(s)$ are the unknown fictitious density distributions on the boundary. $U(s, x)$ is the

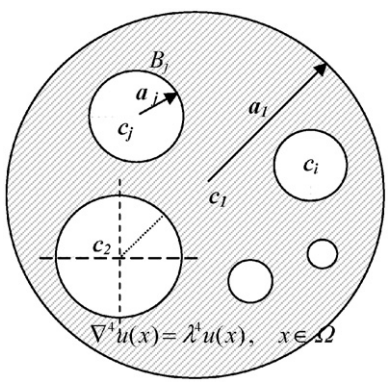


Fig. 1. Problem statement for an eigenproblem with multiple circular holes.

fundamental solution in Eq. (3) and the other three kernels, $\Theta(s, x)$, $M(s, x)$ and $V(s, x)$, can be obtained by applying the following operators defined by

$$K_{\Theta} = \frac{\partial(\cdot)}{\partial n}, \tag{5}$$

$$K_M = \nu\nabla^2(\cdot) + (1-\nu)\frac{\partial^2(\cdot)}{\partial n^2}, \tag{6}$$

$$K_V = \frac{\partial}{\partial n}\nabla^2(\cdot) + (1-\nu)\frac{\partial}{\partial t}\left[\frac{\partial}{\partial n}\left(\frac{\partial}{\partial t}(\cdot)\right)\right] \tag{7}$$

to the kernel $U(s, x)$ with respect to the source point, where $\partial/\partial n$ and $\partial/\partial t$ are the normal and tangential derivatives, respectively. In the polar coordinate of $(R, \theta)$, the normal and tangential derivatives can be expressed by $\partial/\partial R$ and $(1/R)(\partial/\partial\theta)$, respectively, and then the three kernel functions can be rewritten as

$$\Theta(s, x) = K_{\Theta}(U(s, x)) = \frac{\partial U(s, x)}{\partial R}, \tag{8}$$

$$M(s, x) = K_M(U(s, x)) = \nu\nabla^2 U(s, x) + (1-\nu)\frac{\partial^2 U(s, x)}{\partial R^2}, \tag{9}$$

$$V(s, x) = K_V(U(s, x)) = \frac{\partial}{\partial R}\left(\nabla^2 U(s, x)\right) + (1-\nu)\left(\frac{1}{R}\right)\frac{\partial}{\partial\theta}\left[\frac{\partial}{\partial R}\left(\frac{1}{R}\frac{\partial U(s, x)}{\partial\theta}\right)\right]. \tag{10}$$

Since the kernels $P(s, x)$ and $Q(s, x)$ can be selected from any two of the four kernels, $U(s, x)$, $\Theta(s, x)$, $M(s, x)$ and $V(s, x)$, six $(C_2^4)$ formulations can be considered. According to the result of Ref. [26], any combination of kernel can yield the acceptable results. However, the higher the layer potential is chosen, the lower the convergence rate is obtained. More computation is required for using more higher-layer kernel so that the computational efficiency is decreasing. For simplicity, the kernels $U(s, x)$ and $\Theta(s, x)$ are chosen as $P(s, x)$ and $Q(s, x)$ in Eq. (4). In addition to the displacement, the slope, normal moment and effective shear force can be derived by applying the three operators in Eqs. (5)–(7) to Eq. (4) with respect to the field point. Then, the indirect boundary integral representations of the displacement, slope, moment and effect shear force are expressed as follows:

$$u(x) = \int_B U(s, x)\varphi(s)\,\mathrm{d}B(s) + \int_B \Theta(s, x)\psi(s)\,\mathrm{d}B(s), \quad x \in \Omega, \tag{11}$$

$$\theta(x) = \int_B U_{\theta}(s, x)\varphi(s)\,\mathrm{d}B(s) + \int_B \Theta_{\theta}(s, x)\psi(s)\,\mathrm{d}B(s), \quad x \in \Omega, \tag{12}$$

$$m(x) = \int_B U_m(s, x)\varphi(s)\,\mathrm{d}B(s) + \int_B \Theta_m(s, x)\psi(s)\,\mathrm{d}B(s), \quad x \in \Omega, \tag{13}$$

$$v(x) = \int_B U_v(s, x)\varphi(s)\,\mathrm{d}B(s) + \int_B \Theta_v(s, x)\psi(s)\,\mathrm{d}B(s), \quad x \in \Omega. \tag{14}$$

By applying the field point $x$ to the boundary using appropriate expression of degenerate kernel, we have the indirect BIEs for boundary points. For the clamped case, the lateral displacement $u(x)$ and the slope $\theta(x)$ on the boundary are specified to zero. For the free case, the normal moment $m(x)$ and effective shear force $v(x)$ on the boundary are set to zero. The simply supported condition can be obtained by specifying both the lateral displacement $u(x)$ and the normal moment $m(x)$ to zero.

### 2.3. Degenerate kernels and Fourier series for the fictitious boundary densities

In the polar coordinate, the field point and source point can be expressed as $x = (\rho, \phi)$ and $s = (R, \theta)$, respectively. By employing the separation technique for the source and field points, the kernel functions $U(s, x)$ and $\Theta(s, x)$ are expanded in the series form as follows [27]:

$$U: \begin{cases} U^I(s,x) = \frac{1}{8\lambda^2}\sum_{m=0}^{\infty}\varepsilon_m\{J_m(\lambda\rho)[Y_m(\lambda R)+iJ_m(\lambda R)]+\frac{2}{\pi}I_m(\lambda\rho)[K_m(\lambda R)+i(-1)^m I_m(\lambda R)]\} \\ \qquad \times\cos[m(\theta-\phi)], \quad \rho<R \\ U^E(s,x) = \frac{1}{8\lambda^2}\sum_{m=0}^{\infty}\varepsilon_m\{J_m(\lambda R)[Y_m(\lambda\rho)+iJ_m(\lambda\rho)]+\frac{2}{\pi}I_m(\lambda R)[K_m(\lambda\rho)+i(-1)^m I_m(\lambda\rho)]\} \\ \qquad \times\cos[m(\theta-\phi)], \quad \rho\geqslant R \end{cases} \tag{15}$$

$$\Theta: \begin{cases} \Theta^I(s,x) = \frac{1}{8\lambda}\sum_{m=0}^{\infty}\varepsilon_m\{J_m(\lambda\rho)[Y'_m(\lambda R)+iJ'_m(\lambda R)]+\frac{2}{\pi}I_m(\lambda\rho)[K'_m(\lambda R)+i(-1)^m I'_m(\lambda R)]\} \\ \qquad \times\cos[m(\theta-\phi)], \quad \rho<R \\ \Theta^E(s,x) = \frac{1}{8\lambda}\sum_{m=0}^{\infty}\varepsilon_m\{J'_m(\lambda R)[Y_m(\lambda\rho)+iJ_m(\lambda\rho)]+\frac{2}{\pi}I'_m(\lambda R)[K_m(\lambda\rho)+i(-1)^m I_m(\lambda\rho)]\} \\ \qquad \times\cos[m(\theta-\phi)], \quad \rho>R \end{cases} \tag{16}$$

where $\varepsilon_m$ is the Neumann factor ($\varepsilon_m = 1$, $m = 0$; $\varepsilon_m = 2$, $m = 1,2,\ldots,\infty$) and the superscripts "$I$" and "$E$" denote the interior and exterior cases for $U(s, x)$ and $\Theta(s, x)$ degenerate kernels to distinguish $\rho < R$ and $\rho > R$, respectively, as shown in Fig. 2. The other degenerate kernels $U_\theta(s, x)$, $\Theta_\theta(s, x)$, $U_m(s, x)$, $\Theta_m(s, x)$, $U_v(s, x)$ and $\Theta_v(s, x)$ in the indirect boundary integral equations can be obtained by applying the operators of Eqs. (5)–(7) to the degenerate kernel $U(s, x)$ and $\Theta(s, x)$ in Eqs. (15) and (16) with respect to the field point $x$.

In order to fully utilize the geometry of circular boundary, the fictitious boundary densities, $\phi(s)$ and $\psi(s)$, can be expanded by employing the Fourier series. Therefore, we obtain

$$\phi(s) = a_0 + \sum_{m=0}^{\infty}(a_m \cos m\theta + b_m \sin m\theta), \quad s \in B, \tag{17}$$

$$\psi(s) = p_0 + \sum_{m=0}^{\infty}(p_m \cos m\theta + p_m \sin m\theta), \quad s \in B, \tag{18}$$

where $a_0$, $a_m$, $b_m$, $p_0$, $p_m$ and $q_m$ are the Fourier coefficients and $\theta$ is the polar angle. In the real computation, only the finite $M$ terms are used in the summation of Eqs. (17) and (18).

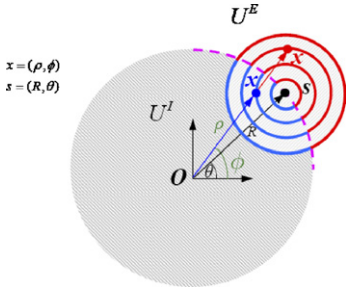


Fig. 2. Degenerate kernel for $U(s, x)$.

## 3. Adaptive observer system and transformation of tensor components

### 3.1. Adaptive observer system

Consider a plate problem with circular boundaries as shown in Fig. 1. Since the indirect boundary integral equations are frame indifferent (i.e. rule of objectivity), the origin of the observer system can be adaptively located on the center of the corresponding boundary contour under integration. Adaptive observer system is chosen to fully employ the circular property by expanding the kernels into degenerate forms. Fig. 3 shows the boundary integration for the circular boundaries in the adaptive observer system. The dummy variable in the circular contour integration is the angle ($\theta$) instead of radial coordinate ($R$). Using the adaptive system, all the boundary integrals can be determined analytically free of principal value senses.

### 3.2. Transformation of tensor components

Since the calculation of the slope, moment and effective shear force are involved in the plate problem, potential gradient or higher-order gradient is required to calculate carefully. For the non-concentric case, special treatment for the potential gradient should be taken care as the source and field points locate on different circular boundaries. As shown in Fig. 4, the angle $\phi_i$ of the collocation point $x_i$ is described in the center of the circle under integration and the angle $\phi_c$ is described in the center of the circle on which collocation point is located. According to the transformation of the component of the vector equation (19) and the tensor equation (20) [28], we have

$$\begin{bmatrix} (\cdot)_n \\ (\cdot)_t \end{bmatrix} = \begin{bmatrix} \cos(\delta) & \sin(\delta) \\ -\sin(\delta) & \cos(\delta) \end{bmatrix} \begin{bmatrix} (\cdot)_r \\ (\cdot)_\theta \end{bmatrix}, \tag{19}$$

$$\begin{bmatrix} (\cdot)_{nn} \\ (\cdot)_{nt} \end{bmatrix} = \begin{bmatrix} \cos^2(\delta) & \sin^2(\delta) & 2\sin(\delta)\cos(\delta) \\ -\sin(\delta)\cos(\delta) & \sin(\delta)\cos(\delta) & \cos^2(\delta) - \sin^2(\delta) \end{bmatrix} \begin{bmatrix} (\cdot)_{rr} \\ (\cdot)_{\theta\theta} \\ (\cdot)_{r\theta} \end{bmatrix}. \tag{20}$$

The three operators in Eqs. (5)–(7) can be transformed as follows:

$$K_\Theta^R = \cos(\delta)\frac{\partial(\cdot)}{\partial n} + \sin(\delta)\frac{\partial(\cdot)}{\partial t}, \tag{21}$$

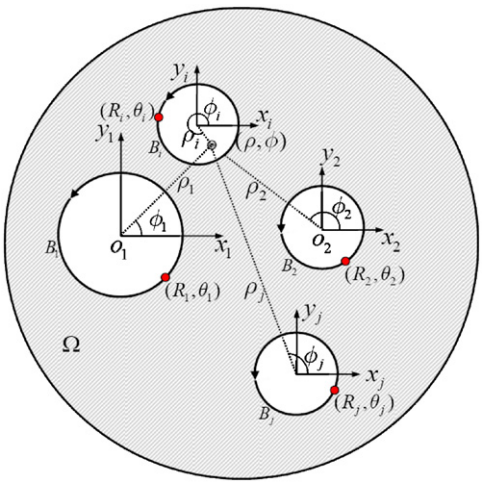


Fig. 3. Adaptive observer system when integrating the corresponding circular boundaries.

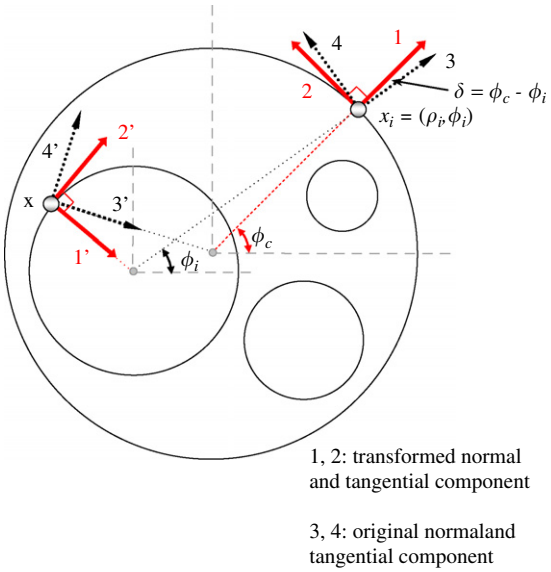


Fig. 4. Transformation of tensor components.

$$K_M^R = \left[v + (1-v)\sin^2(\delta)\right]\nabla^2(\cdot) + \cos(2\delta)(1-v)\frac{\partial^2(\cdot)}{\partial n^2} + \sin(2\delta)(1-v)\frac{\partial}{\partial n}\left(\frac{\partial(\cdot)}{\partial t}\right), \tag{22}$$

$$\begin{aligned} K_V^R = {} & \cos(\delta)\frac{\partial}{\partial n}\nabla^2(\cdot) + \sin(\delta)(1+(1-v)\cos(\delta))\frac{\partial}{\partial t}\nabla^2(\cdot) \\ & - \sin(2\delta)(1-v)\frac{\partial}{\partial t}\left[\frac{\partial^2}{\partial n^2}(\cdot)\right] + \cos(2\delta)(1-v)\frac{\partial}{\partial t}\left[\frac{\partial}{\partial n}\left(\frac{\partial}{\partial t}(\cdot)\right)\right], \end{aligned} \tag{23}$$

where $\delta = \phi_c - \phi_i$. When the angle $\phi_c$ equals to the angle $\phi_i$ or the angle difference $\delta$ equals to zero, Eqs. (21)–(23) are simplified to the Eqs. (5)–(7). Considering non-concentric cases, the degenerate kernels, $U_\theta(s, x)$, $\Theta_\theta(s, x)$, $U_m(s, x)$, $\Theta_m(s, x)$, $U_v(s, x)$, and $\Theta_v(s, x)$, can be obtained by applying the operators of Eqs. (21)–(23) to the degenerate kernel $U(s, x)$ and $\Theta(s, x)$ in Eqs. (15) and (16) with respect to the field point $x$. The explicit forms of these degenerate kernels are listed in Appendix A.

## 4. Linear algebraic system

Consider the plate problem with circular domain containing $H$ randomly distributed circular holes centered at the position vector $\boldsymbol{c}_j$ ($j = 1, 2, \ldots, L$), ($L = 1 + H$ and $\boldsymbol{c}_1$ is the position vector of the outer circular boundary for the plate), as shown in Fig. 5 in which $R_j$ denotes the radius of the $j$th circular region, $x_j$ is the collocation point and $B_j$ is the boundary of the $j$th circular hole. By uniformly collocating the $N(= 2M+1)$ collocation points on each circular boundary in Eqs. (11)–(14), we have

$$u(x) = \sum_{j=1}^{L}\int_{B_j}\left\{U(s,x)\phi(s) + \Theta(s,x)\psi(s)\right\}\mathrm{d}B_j(s), \quad x \in B, \tag{24}$$

$$\theta(x) = \sum_{j=1}^{L}\int_{B_j}\left\{U_\theta(s,x)\phi(s) + \Theta_\theta(s,x)\psi(s)\right\}\mathrm{d}B_j(s), \quad x \in B, \tag{25}$$

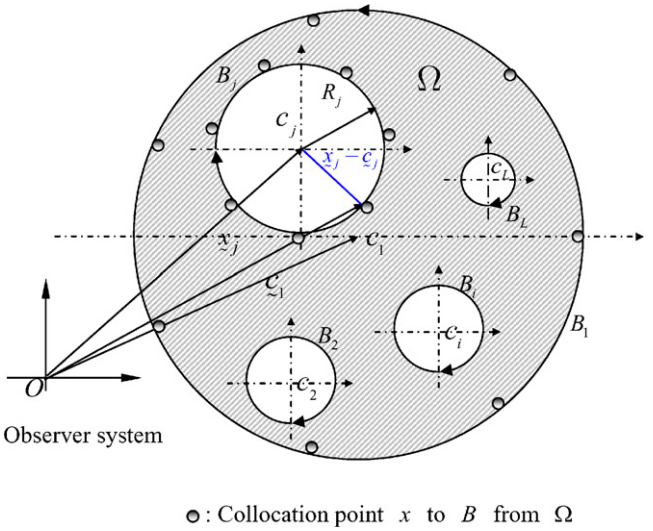


Fig. 5. Collocation point and boundary contour integration in the boundary integral equation.

$$m(x) = \sum_{j=1}^{L} \int_{B_j} \left\{ U_m(s,x)\phi(s) + \Theta_m(s,x)\psi(s) \right\} \mathrm{d}B_j(s), \quad x \in B, \tag{26}$$

$$v(x) = \sum_{j=1}^{L} \int_{B_j} \left\{ U_v(s,x)\phi(s) + \Theta_v(s,x)\psi(s) \right\} \mathrm{d}B_j(s), \quad x \in B. \tag{27}$$

It must be noted that $U$, $\Theta$, $U_\theta$, $\Theta_\theta$ and $U_m$ are weakly singular, $\Theta_m$ and $U_v$ are singular and $\Theta_v$ is hypersingular [29] since $x$ and $s$ may coincide. The main gain by using degenerate kernel in the BIE is that singular integrals due to the kernels can be transformed to series sum free of facing principal values. The selection of interior or exterior degenerate kernel depends on $\rho > R$ or $\rho < R$, respectively, according to the observer system. For the $B_j$ integral of circular boundary, the degenerate kernels of $U(s, x)$, $\Theta(s, x)$, $U_\theta(s, x)$, $\Theta_\theta(s, x)$, $U_m(s, x)$, $\Theta_m(s, x)$, $U_v(s, x)$ and $\Theta_v(s, x)$ are utilized while the fictitious boundary density $\phi(s)$ and $\psi(s)$ along the circular boundary are substituted by using the Fourier series of Eqs. (17) and (18), respectively. In the $B_j$ integration, the origin of the observer system is adaptively set to collocate at the center $c_j$ to utilize the degenerate kernels and Fourier series. By considering the outer circular boundary clamped and inner circular boundary free as an example, a linear algebraic system can be written due to orthogonal property as follows:

$$\begin{bmatrix} U^{11} & \Theta^{11} & U^{12} & \Theta^{12} & \cdots & U^{1L} & \Theta^{1L} \\ U_\theta^{11} & \Theta_\theta^{11} & U_\theta^{12} & \Theta_\theta^{12} & \cdots & U_\theta^{1L} & \Theta_\theta^{1L} \\ U_m^{21} & \Theta_m^{21} & U_m^{22} & \Theta_m^{22} & \cdots & U_m^{2L} & \Theta_m^{2L} \\ U_v^{21} & \Theta_v^{21} & U_v^{22} & \Theta_v^{22} & \cdots & U_v^{2L} & \Theta_v^{2L} \\ \vdots & \vdots & \vdots & \vdots & \ddots & \vdots & \vdots \\ U_m^{L1} & \Theta_m^{L1} & U_m^{L2} & \Theta_m^{L2} & \cdots & U_m^{LL} & \Theta_m^{LL} \\ U_v^{L1} & \Theta_v^{L1} & U_v^{L2} & \Theta_v^{L2} & \cdots & U_v^{LL} & \Theta_v^{LL} \end{bmatrix} \begin{Bmatrix} \Phi^1 \\ \Psi^1 \\ \Phi^2 \\ \Psi^2 \\ \vdots \\ \Phi^L \\ \Psi^L \end{Bmatrix} = \begin{Bmatrix} 0 \\ 0 \\ 0 \\ 0 \\ \vdots \\ 0 \\ 0 \end{Bmatrix}, \tag{28}$$

where $L$ denotes the number of circular boundaries (including inner and outer circular boundaries). For brevity, a unified form $[U^{ij}]$ ($i = 1,2,3,\ldots,L$ and $j = 1,2,3,\ldots,L$) denote the response of $U(s, x)$ kernel at the $i$th

circle point due to the source at the $j$th circle. Otherwise, the same definition is for $[\Theta^{ij}]$, $[U_\theta^{ij}]$, $[\Theta_\theta^{ij}]$, $[U_m^{ij}]$, $[\Theta_m^{ij}]$, $[U_v^{ij}]$ and $[\Theta_v^{ij}]$ kernels. The explicit expressions for sub-vectors $[\Phi^i]$ and $[\Psi^i]$ can be described as follows:

$$\Phi^i = \begin{Bmatrix} a_0^i \\ a_1^i \\ b_1^i \\ \vdots \\ a_M^i \\ b_M^i \end{Bmatrix} \quad \Psi^i = \begin{Bmatrix} p_0^i \\ p_1^i \\ q_1^i \\ \vdots \\ p_M^i \\ q_M^i \end{Bmatrix}. \tag{29}$$

The explicit expressions for the sub-matrices of $[U^{ij}]$, $[\Theta^{ij}]$, $[U_\theta^{ij}]$, $[\Theta_\theta^{ij}]$, $[U_m^{ij}]$, $[\Theta_m^{ij}]$, $[U_v^{ij}]$ and $[\Theta_v^{ij}]$ can be obtained through replacing $K$ in Eq. (30) by $U$, $\Theta$, $U_\theta$, $\Theta_\theta$, $U_m$, $\Theta_m$, $U_v$ and $\Theta_v$,

$$K^{ij} = \begin{bmatrix} K_{0C}^{ij}(\rho_1,\phi_1) & K_{1C}^{ij}(\rho_1,\phi_1) & K_{1S}^{ij}(\rho_1,\phi_1) & \cdots & K_{MS}^{ij}(\rho_1,\phi_1) \\ K_{0C}^{ij}(\rho_2,\phi_2) & K_{1C}^{ij}(\rho_2,\phi_2) & K_{1S}^{ij}(\rho_2,\phi_2) & \cdots & K_{MS}^{ij}(\rho_2,\phi_2) \\ \vdots & \vdots & \vdots & & \vdots \\ \vdots & \vdots & \vdots & & \vdots \\ K_{0C}^{ij}(\rho_N,\phi_N) & K_{1C}^{ij}(\rho_N,\phi_N) & K_{1S}^{ij}(\rho_N,\phi_N) & \cdots & K_{MS}^{ij}(\rho_N,\phi_N) \end{bmatrix}_{N\times N}, \tag{30}$$

where $\phi_k$ and $\rho_k (k = 1, 2, 3,\ldots,N)$ are the $k$th collocation angle and radius of the collocation point on each boundary in the observer system and the element of the sub-matrices can be integrated by

$$K_{nC}^{ij}(\rho_i,\phi_i) = \int_0^{2\pi} K(R,\theta;\rho_i,\phi_i)\cos(n\theta)(R\,\mathrm{d}\theta), \quad n = 0,1,2,\ldots,M, \tag{31}$$

$$K_{nS}^{ij}(\rho_i,\phi_i) = \int_0^{2\pi} K(R,\theta;\rho_i,\phi_i)\sin(n\theta)(R\,\mathrm{d}\theta), \quad n = 1,2,\ldots,M \tag{32}$$

in which the interior degenerate kernels are used for $j = 1$, $i = 1, 2, 3,\ldots,N$; otherwise, exterior degenerate kernels are used. According to the direct-searching scheme, the eigenvalues can be obtained by applying the SVD [30] technique to the matrix in the left-hand side of Eq. (28). Once the eigenvalues are obtained, the associated mode shape can be obtained by substituting the corresponding eigenvectors (i.e. the Fourier series representing the fictitious boundary density) into the indirect boundary integral representation. The procedure of solution is described in a flowchart as shown in Fig. 6.

## 5. Numerical results and discussions

### 5.1. Case 1: an annular plate [1,14]

An annular plate with the outer radius of one meter ($a = 1$ m), the inner radius of 0.25 m ($b = 0.25$ m), thickness of 0.002 m and the Poisson ratio $v = 1/3$ are considered as shown in Fig. 7. The outer and inner boundaries are subject to the clamped and free boundary conditions, respectively. Figs. 8(a) and (b) show the first and the second minimum singular values of the influence matrix of Eq. (28) versus the frequency parameter $\lambda$. Since the direct-searching scheme is used, the drop location indicates the eigenvalue. The simultaneous appearance of drop indicates the multiplicities as given in Fig. 8(b). The annular case was also solved by using the FEM software (ABAQUS) [31] with 8903 elements and 9099 nodes. The general-purpose shell elements, S4, of ABAQUS were used to model the plate problem. Although the thickness of the plate is 0.002 m, these elements do not suffer from transverse shear locking based on the theory manual of

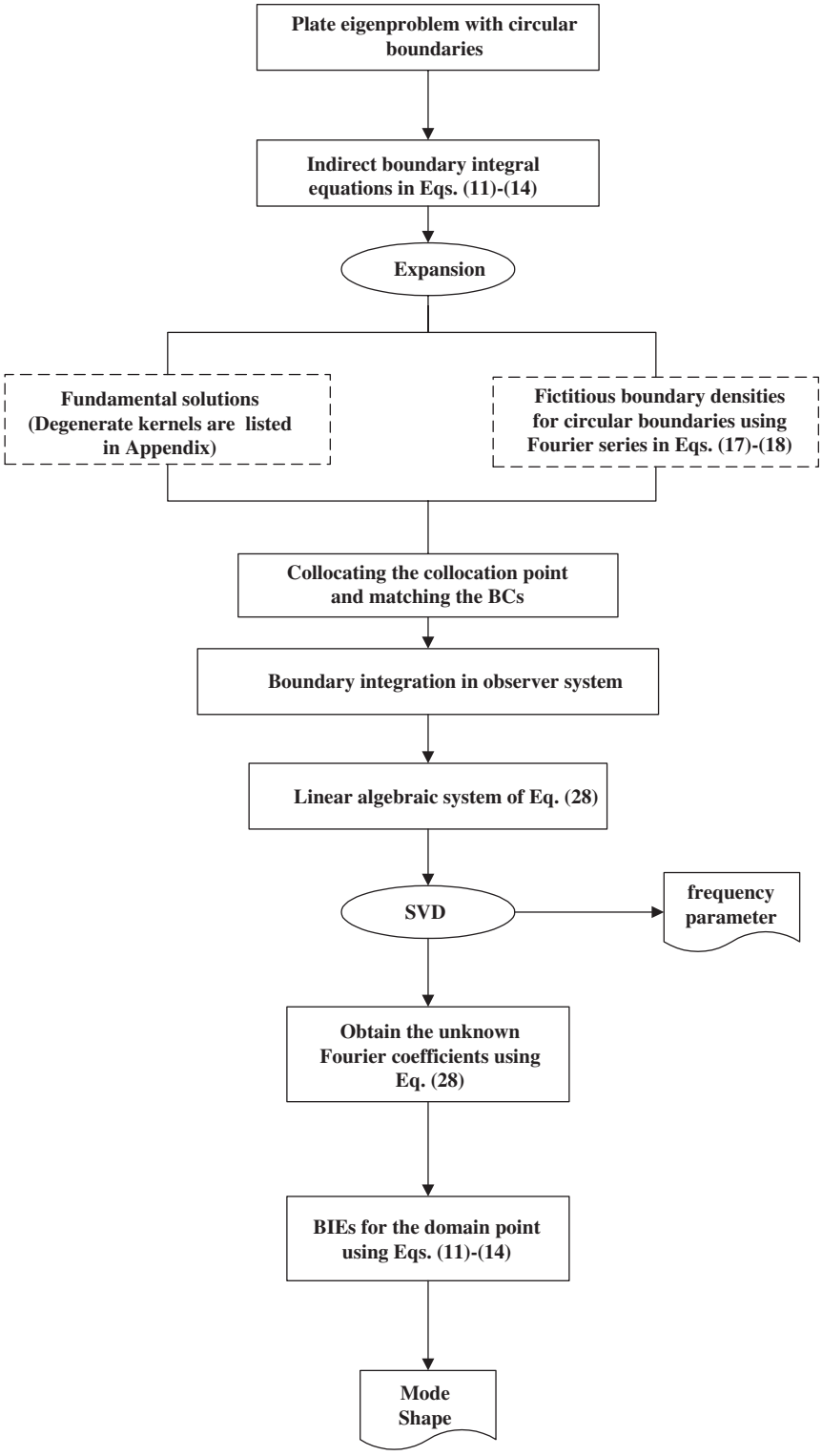


Fig. 6. Flowchart of the present method.

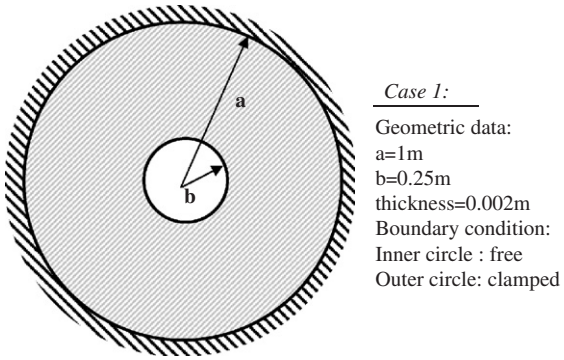


Fig. 7. An annular plate with clamped–free boundary condition.

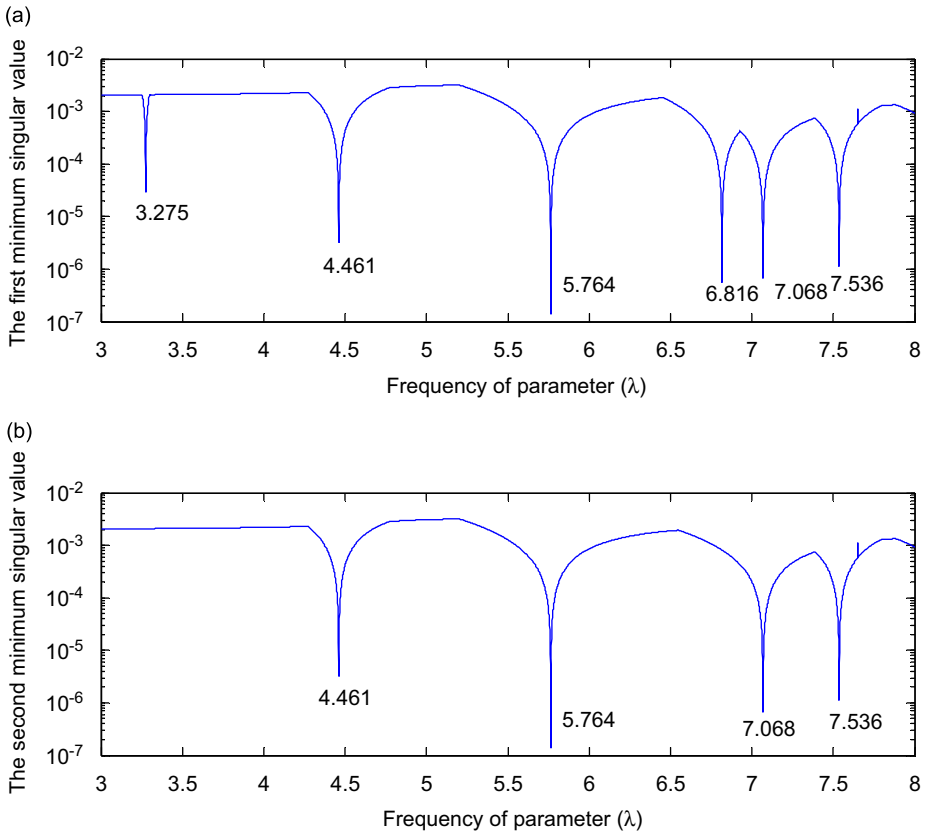


Fig. 8. The first and the second minimum singular values versus the frequency parameter for an annular plate ($a = 1.0$, $b = 0.25$).

ABAQUS [31]. The unknown fictitious boundary densities of the plate are represented in terms of Fourier series. The former six natural frequency parameters versus the number of degrees of freedom of two methods for an annular plate are shown in Fig. 9. The number of degrees of freedom of the present method is $q = 2(2M+1)$ where $M$ is the number of terms of Fourier series. The number of scaling degrees of freedom of the FEM is $\mathrm{sd} = 2\ln(x)$ where $x$ (6 times the number of nodes) is the total number of degrees of freedom for the finite element model. Actually, the value of $x$ ranges from 96 to 7722 in the case. In order to achieve the same accuracy to the analytic solution, the required number of degrees of freedom by using the present method is much less than that of the FEM. Consequently, the computational efficiency and convergence of the present method over FEM is obvious. It is found that some modes such as third and fifth mode are lost when

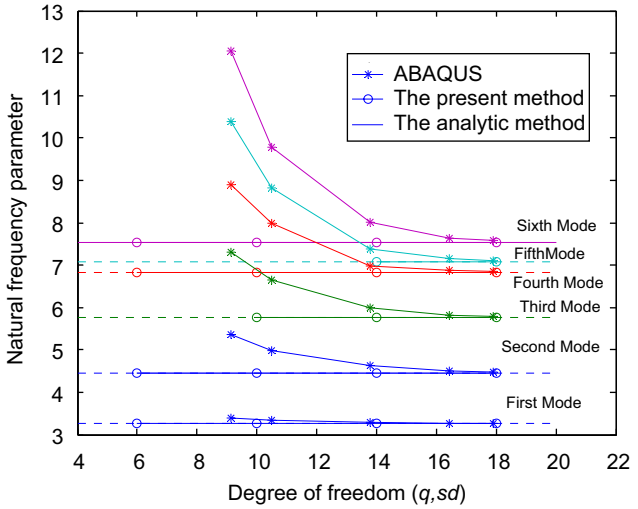


Fig. 9. Natural frequency parameter versus the number of degrees of freedom of two methods for an annular plate ($a = 1.0$, $b = 0.25$).

| MODE | 1 | 2 | 3 | 4 | 5 | 6 |
|---|---|---|---|---|---|---|
| Present method | 3.2750 | 4.4610* | 5.7640* | 6.8160 | 7.0680* | 7.5360* |
| | 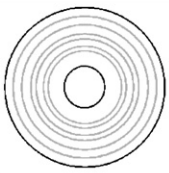 | 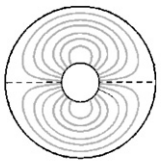 |  |  | 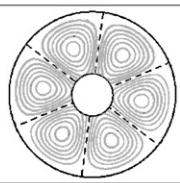 | 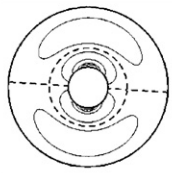 |
| ABAQUS | 3.2747 | 4.4631* | 5.7676* | 6.8201 | 7.0736* | 7.5427* |
| | 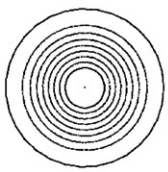 | 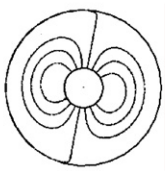 | 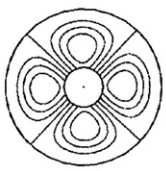 | 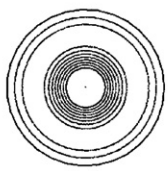 | 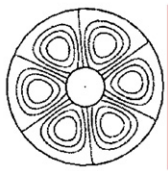 | 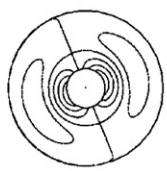 |
| Khurasia and Rawtani [1] | 3.1623 | 4.4159 | 5.5678 | 6.7823 | 6.9138 | N/A |
| | <2.9155> | <4.1593> | <5.2915> | <6.4807> | N/A | N/A |
| | N/A | 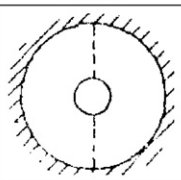 | 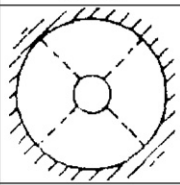 | 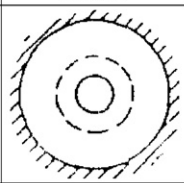 | 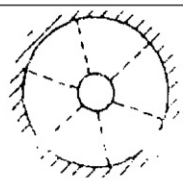 | N/A |
| Exact[14] | 3.2719 | 4.4623 | 5.7640 | 6.8183 | 7.0680 | 7.5391 |

Fig. 10. The former six natural frequency parameters and modes of an annular plate ($a = 1.0$, $b = 0.25$). $\langle\ \rangle$: experimental data [1]; $*$: multiplicity.

only one term ($M = 1$) is involved in the Fourier series. The reason is that the third mode shape, shown in Fig. 9, has two diametrical nodes. The same explanations can be applied to the fifth mode which does not appear until three terms ($M = 3$) are used due to its mode shape with three diametrical nodes. Besides, the number of terms used will influence the number of mode appeared, but the value of natural frequency parameter of the captured mode can be well predicted. From the study of the convergence, only three terms ($M = 3$) in the Fourier series is taken to capture the former sixth modes. Then seven collocation points are required in each circular boundary. Fig. 10 shows the former six natural frequency parameters and modes by

using FEM [1,31], the analytical method [14] and the present method. The results of the present method are good in agreement with the exact solutions and the FEM results using ABAQUS. A slight deviation is shown in the results of Khurasia and Rawtani due to the rough mesh of finite element model.

### 5.2. Case 2: a circular plate with an eccentric hole [1]

A circular plate weakened by an eccentric hole with the same outer and inner radii as the *Case* 1 is considered. The offset distance $e$ of the eccentric hole is 0.45 m ($e/a = 0.45$) as shown in Fig. 11. The former six natural frequency parameters versus the number of degrees of freedom of two methods for the Case 2 are shown in Fig. 12. Following the same treatment in Fig. 9, the scaling degrees of freedom of the FEM is $\mathrm{sd} = 4.5\ln(x)$. All the notations are the same as the Case 1. The total number of degrees of freedom by using the finite element model ranges from 96 to 7686. In this case, the present method still has the feature of high efficiency and fast convergence. Since the point-collocation approach was adopted in this paper, neither upper bound nor lower bound solution can be proved. It shows that the number of terms used influences the natural

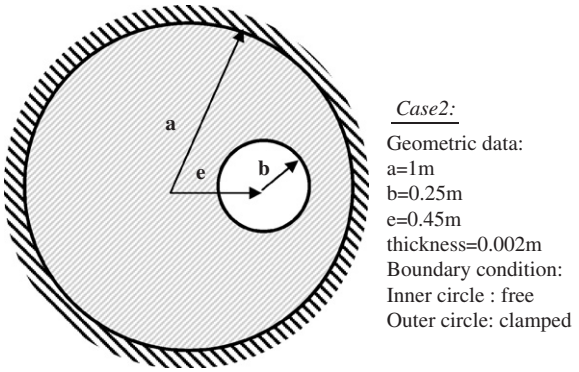


Fig. 11. A circular plate with an eccentric hole in clamped–free boundary condition.

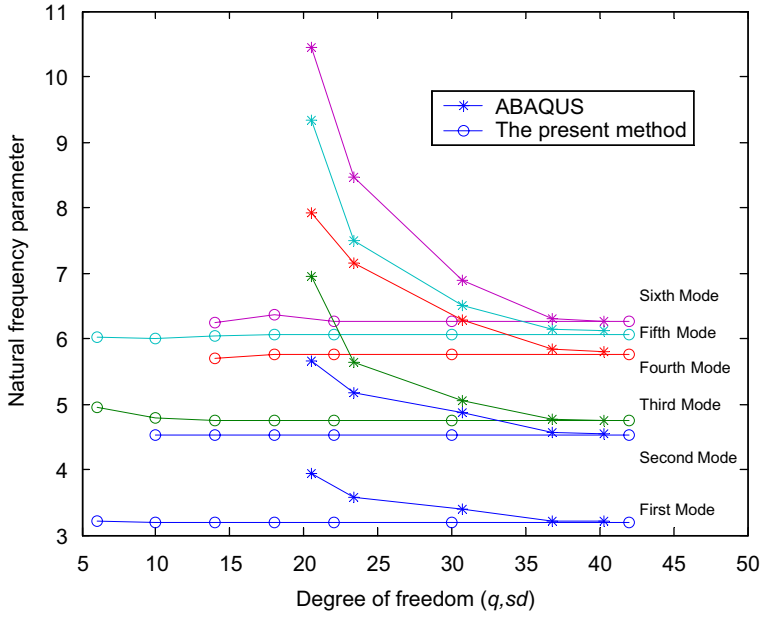


Fig. 12. Natural frequency parameter versus the number of degrees of freedom of two methods for a circular plate with an eccentric hole ($a = 1.0$, $b = 0.25$, $e = 0.45$).

frequency parameter as well as the number of mode. Since the induced eccentric hole affects the axial symmetric characteristics, some diametric nodes, e.g. the second, the fourth and the sixth modes, are lost when insufficient terms of Fourier series are used. Fig. 13 indicates the minimum singular value of the influence matrix versus the frequency parameter $\lambda$ using seven terms of Fourier series ($M = 7$). The multiplicity is one only due to the lack of axial symmetry. The FEM model of the ABAQUS used 8217 elements and 8404 nodes.

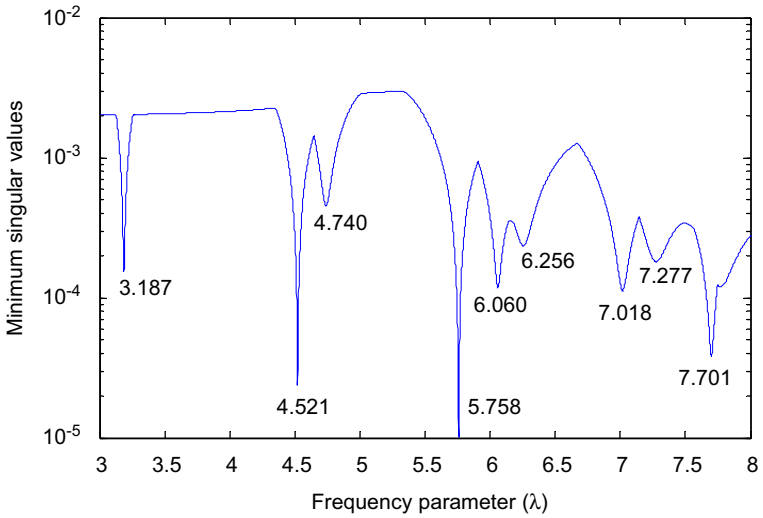


Fig. 13. The minimum singular value versus the frequency parameter for a circular plate with an eccentric hole ($a = 1.0$, $b = 0.25$, $e = 0.45$).

| MODE | 1 | 2 | 3 | 4 | 5 | 6 |
|---|---|---|---|---|---|---|
| Present method | 3.1870 | 4.5210 | 4.7400 | 5.7580 | 6.0600 | 6.2560 |
| | 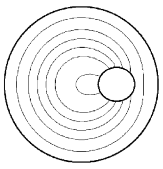 | 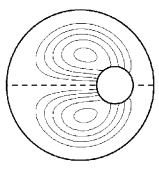 | 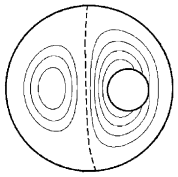 | 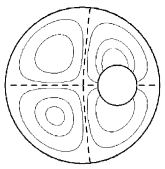 | 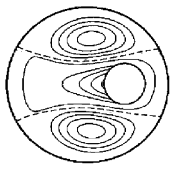 | 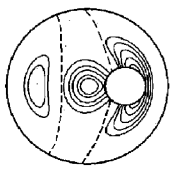 |
| ABAQUS | 3.2020 | 4.5300 | 4.7450 | 5.7753 | 6.0899 | 6.2361 |
| | 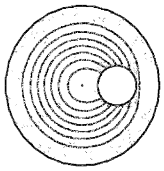 | 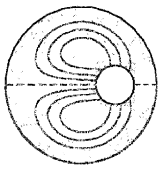 | 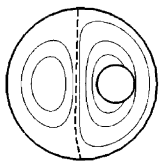 | 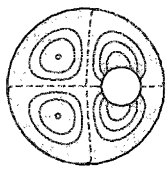 | 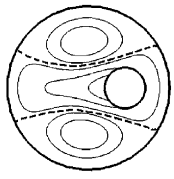 | 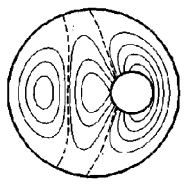 |
| Khurasia and Rawtani [1] | 3.1623 | N/A | 4.6690 | N/A | 5.8138 | 6.0828 |
| | <2.8810> | N/A | <4.6904> | N/A | <5.6391> | N/A |
| | N/A | N/A | 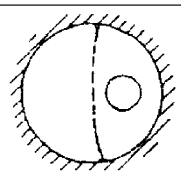 | N/A | 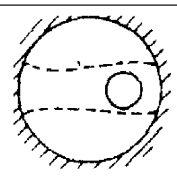 | 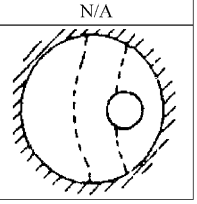 |

Fig. 14. The former six natural frequency parameters and modes of a circular plate with an eccentric hole ($a = 1.0$, $b = 0.25$, $e = 0.45$). $\langle\ \rangle$: experimental data [1].

The former six natural frequency parameters and modes by using FEM [1,31] and the present method are shown in Fig. 14. The results of the present method match well with those of FEM using ABAQUS. In the results of Khurasia and Rawtani [1], the first mode was not reported and the second and fourth modes are lost. An obvious deviation can be seen in the sixth mode of results reported by Khurasia and Rawtani due to the coarse mesh. Our result also agrees well with that of Cheng et al. [11]. Owing to the lack of stiffness of the clamped boundary condition in reality, it is expected that the experimental data [1] are less than those obtained by the other methods.

The effect of eccentricity of $e/a$ versus frequency parameters is shown in Fig. 15 which includes the results of the present method and FEM using ABAQUS for comparison. Good agreement with the data of [11] is also made. The values of $m$ and $n$ in mode $(m, n)$ are the numbers of diametrical and circular nodes, respectively. The repeated frequencies occurring in annular case, i.e. $m \neq 0$, are gradually separated into two distinct values as the variation in eccentricity increases due to initial axial symmetry broken. Considering different boundary conditions, clamped and simply supported at the outer edge, Table 1 lists former six eigenvalues ($\lambda^2$) of circular plate with a circular hole of radius $b/a = 0.4$ and eccentricity $e/a$ changing from 0.1, 0.3 to 0.5. Except

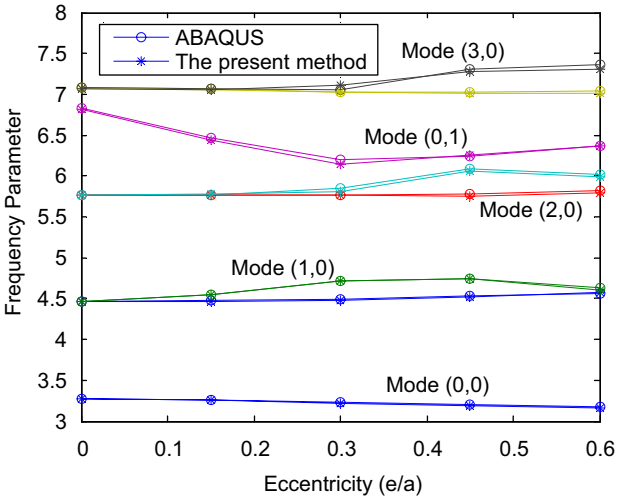


Fig. 15. Effect of variation in $e/a$ on frequency parameters.

Table 1
The former six eigenvalues ($\lambda^2$) for clamped–free and simple supported–free circular plate with a circular hole of radius $b/a = 0.4$ and eccentricity $e/a$ changing from 0.1, 0.3 to 0.5

| Eccentricity | BC | Method | 1 | 2 | 3 | 4 | 5 | 6 |
|---|---|---|---|---|---|---|---|---|
| $e/a = 0.1$ | C–F | 1 | 13.0465 | 19.6249 | 21.0314 | 31.8999 | 31.9451 | 47.1969 |
| | | 2 | 13.0480 | N/A | 21.0260 | N/A | 31.9530 | 47.2310 |
| | S–F | 1 | 4.7524 | 12.0270 | 12.2500 | 23.2131 | 23.2131 | 37.2832 |
| | | 2 | 4.7486 | N/A | 12.2530 | N/A | 23.2180 | 37.2930 |
| $e/a = 0.3$ | C–F | 1 | 11.2359 | 19.8025 | 26.0508 | 34.0356 | 39.2377 | 41.9127 |
| | | 2 | 11.2409 | N/A | 26.0740 | N/A | 39.1730 | 41.6860 |
| | S–F | 1 | 4.6483 | 12.1661 | 14.1075 | 23.6002 | 24.1867 | 31.1364 |
| | | 2 | 4.6454 | N/A | 14.1160 | N/A | 24.2840 | 31.1370 |
| $e/a = 0.5$ | C–F | 1 | 10.1124 | 20.0883 | 24.3838 | 34.5744 | 37.0394 | 43.6921 |
| | | 2 | 10.1420 | N/A | 24.4310 | N/A | 37.0650 | 44.2150 |
| | S–F | 1 | 4.5199 | 12.3904 | 15.3037 | 23.7754 | 27.2484 | 29.5718 |
| | | 2 | 4.5258 | N/A | 15.3100 | N/A | 27.3240 | 29.6200 |

Method 1: The present method.
Method 2: Laura [12].

one of the mode (1,0) and mode (2,0) not given in the Laura's results [12], where only symmetric conditions were considered in their trial functions, the results of the present method match well those of Laura et al. The frequencies of annular-like plate with clamped–free boundary condition are larger than those with simply supported–free cases due to the stiffness of the clamped condition. No matter what boundary conditions are at outer edge, the split of repeated frequencies always exists and the difference between two values becomes obvious as eccentricity increases.

### 5.3. Case 3: a circular plate with two holes

In order to demonstrate the generality of the present method, a circular plate with two holes is considered as shown in Fig. 16. The radii of holes are 0.25 and 0.15 m and the coordinates of the center are (0.5,0) and

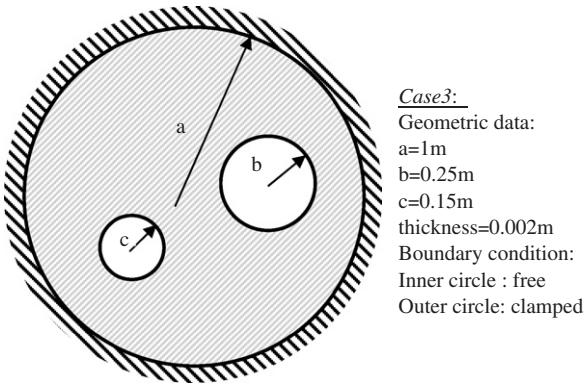


Fig. 16. A circular plate with two circular holes in clamped–free boundary condition.

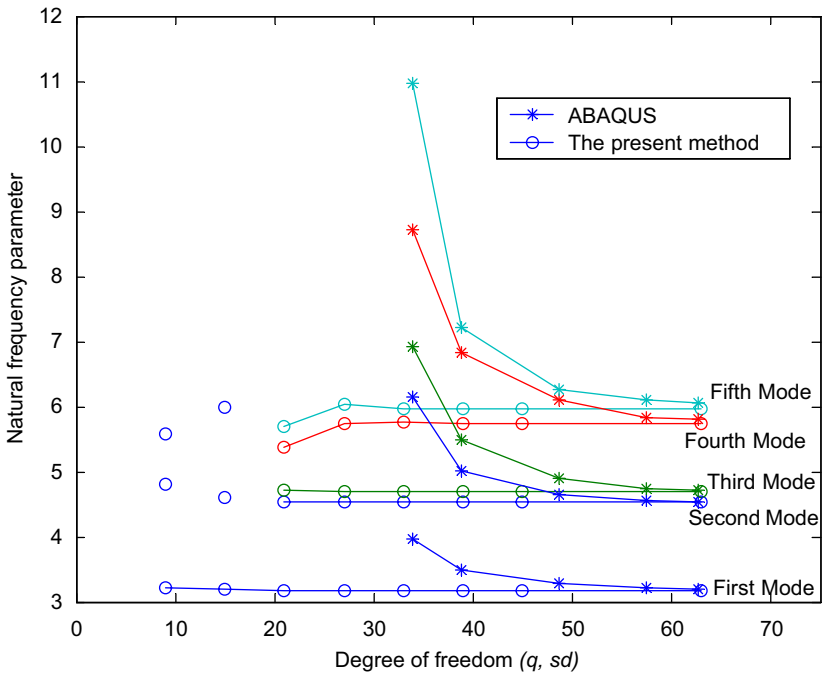


Fig. 17. Natural frequency parameter versus the number of degrees of freedom of two methods for a circular plate with two holes ($a = 1.0$, $b = 0.25$, $c = 0.15$).

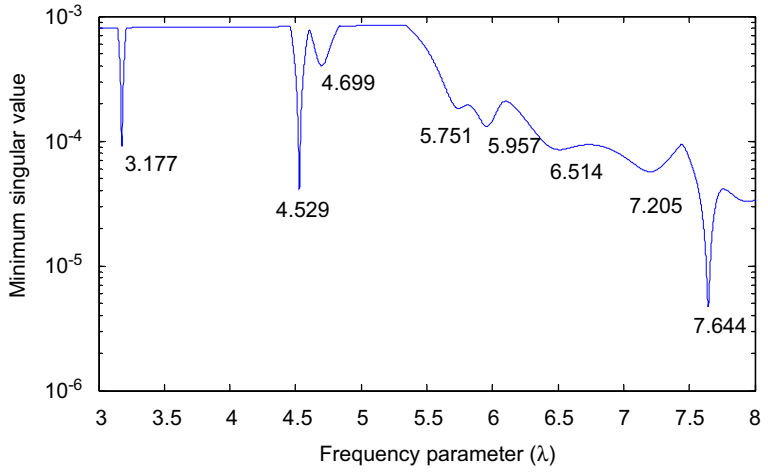


Fig. 18. The minimum singular value versus the frequency parameter for a circular plate with two holes ($a = 1.0$, $b = 0.25$, $c = 0.15$).

| MODE | 1 | 2 | 3 | 4 | 5 |
|---|---|---|---|---|---|
| Present method | 3.1770 | 4.5290 | 4.699 | 5.7510 | 5.9570 |
| | 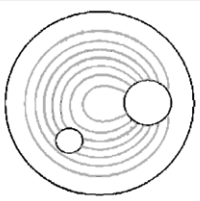 | 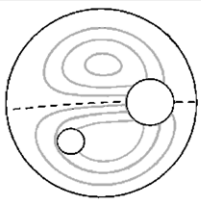 | 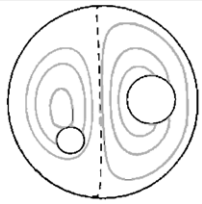 | 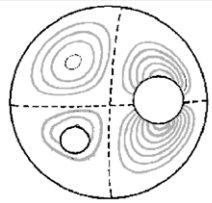 | 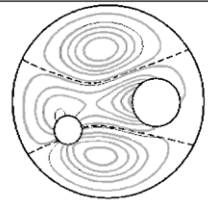 |
| ABAQUS | 3.1950 | 4.5296 | 4.7086 | 5.8070 | 6.0280 |
| | 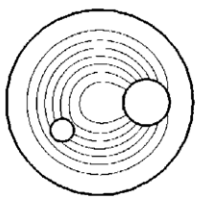 | 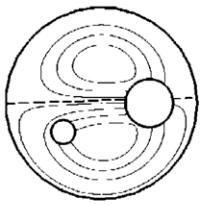 | 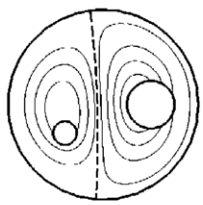 | 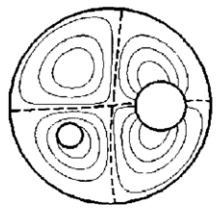 | 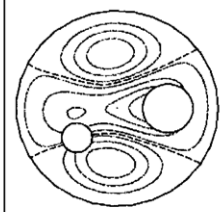 |

Fig. 19. The former five natural frequency parameters and modes of a circular plate with two holes ($a = 1.0$, $b = 0.25$, $c = 0.15$).

$(-0.4,-0.3)$, respectively, in the coordinate system with origin at the center of outer circle. The former five natural frequency parameters versus degrees of freedom of two methods for this case are shown in Fig. 17. The number of degrees of freedom of the present method is $q = 3(2M+1)$ and that of the FEM is $\mathrm{sd} = 7\ln(x)$, where definitions of $M$ and $x$ are the same as the Case 1. The total number of degrees of freedom of the finite element model ranges from 126 to 7836. When the number of inner circular hole increases, the high efficiency can also be observed. Owning to the complex geometrical configuration, the fewer terms of Fourier series ($M = 1$ or 2) cannot capture the second and higher natural frequencies of parameters well. Fig. 18 shows the minimum singular value of the influence matrix versus the frequency parameter $\lambda$ where the number of Fourier series terms $M$ is taken as 7. Fig. 19 shows the former five natural frequency parameters and modes of FEM using ABAQUS and the present method. Good agreement between the results of the present method and those of ABAQUS is obtained.

## 6. Concluding remarks

A semi-analytical approach for solving the natural frequencies and natural modes for the circular plate with multiple circular holes was proposed. Instead of employing the direct formulation, the present method used indirect boundary integral equations in conjugation with the degenerate kernels and the Fourier series to represent the fictitious boundary densities in the adaptive observer system. The improper integrals in the indirect BIEs were avoided by employing the degenerate kernels and were easily calculated through the series sum. The potential across the circular boundary was described explicitly by the interior and exterior expressions of degenerate kernels. The degenerate kernels of the slope, moment and effective shear force in the plate eigenproblems have been derived. Once the Fourier coefficients of fictitious boundary densities have been determined, the corresponding mode shape can be obtained by using the indirect boundary integral representation. The effect of eccentricity of the hole on the natural frequencies is considered. The natural frequencies and corresponding mode shapes for the multiply-connected plate problems with circular boundaries and multiple circular holes have been solved easily and efficiently by using the present method in comparison with the available exact solutions and FEM results using ABAQUS.

## Appendix A. Degenerate kernels

$$U^I(x,s)=\sum_{m=0}^{\infty} f_1\cos(m(\theta-\phi_i))$$

$$\text{where } f_1=\frac{1}{8\lambda^2}\varepsilon_m\left\{J_m(\lambda\rho)[Y_m(\lambda R)+iJ_m(\lambda R)]+\frac{2}{\pi}I_m(\lambda\rho)[K_m(\lambda R)+i(-1)^m I_m(\lambda R)]\right\},$$

$$U^E(x,s)=\sum_{m=0}^{\infty} f_2\cos(m(\theta-\phi_i))$$

$$\text{where } f_2=\frac{1}{8\lambda^2}\varepsilon_m\left\{J_m(\lambda R)[Y_m(\lambda\rho)+iJ_m(\lambda\rho)]+\frac{2}{\pi}I_m(\lambda R)[K_m(\lambda\rho)+i(-1)^m I_m(\lambda\rho)]\right\},$$

$$\Theta^I(x,s)=\frac{\partial U^1(x,s)}{\partial R}=\sum_{m=0}^{\infty} g_1\cos(m(\theta-\phi))$$

$$\text{where } g_1=\frac{1}{8\lambda}\varepsilon_m\left\{J_m(\lambda\rho)[Y'_m(\lambda R)+iJ'_m(\lambda R)]+\frac{2}{\pi}I_m(\lambda\rho)[K'_m(\lambda R)+i(-1)^m I'_m(\lambda R)]\right\},$$

$$\Theta^E(x,s)=\frac{\partial U^2(x,s)}{\partial R}=\sum_{m=0}^{\infty} g_2\cos(m(\theta-\phi))$$

$$\text{where } g_2=\frac{1}{8\lambda}\varepsilon_m\left\{J'_m(\lambda R)[Y_m(\lambda\rho)+iJ_m(\lambda\rho)]+\frac{2}{\pi}I'_m(\lambda R)[K_m(\lambda\rho)+i(-1)^m I_m(\lambda\rho)]\right\},$$

$$\varepsilon_m=\begin{cases}1 & m=0,\\ 2 & m\neq 0.\end{cases}$$

Superscripts $I$ and $E$ denote the interior domain (i.e. $\rho<R$) and exterior domain (i.e. $\rho>R$), respectively:

$$U^K_\theta(x,s)=\sum_{m=0}^{\infty} c_1 f'_K\cos(m(\theta-\phi_i))+s_0 f_K\sin(m(\theta-\phi_i)),\quad k=1,2,$$

$$\Theta^K_\theta(x,s)=\sum_{m=0}^{\infty} c_1 g'_K\cos(m(\theta-\phi_i))+s_0 g_K\sin(m(\theta-\phi_i)),\quad k=1,2,$$

$$c_1 = \cos(\delta_i), \quad s_0 = \left(\frac{m}{\rho_i}\right)\sin(\delta_i),$$

$$U_m^K(x,s) = \sum_{m=0}^{\infty}[mc_0 f_K + mc_1 f'_K + mc_2 f''_K]\cos(m(\theta-\phi_i)) + [ms_0 f_K + ms_1 f'_K]\sin(m(\theta-\phi_i)),$$

$$\Theta_m^K(x,s) = \sum_{m=0}^{\infty}[mc_0 g_K + mc_1 g'_K + mc_2 g''_K]\cos(m(\theta-\phi_i)) + [ms_0 g_K + ms_1 g'_K]\sin(m(\theta-\phi_i)), \quad k = 1,2,$$

$$mc_0 = -\left(\frac{m^2}{2\rho_i^2}\right)(1+v+(-1+v)\cos(2\delta_i)), \quad ms_0 = \left(\frac{m}{\rho_i^2}\right)(-1+v)\sin(2\delta_i),$$

$$mc_1 = \left(\frac{1}{2\rho_i}\right)(1+v+(-1+v)\cos(2\delta_i)), \quad ms_1 = \left(\frac{m}{\rho_i}\right)(1-v)\sin(2\delta_i),$$

$$mc_2 = \left(\frac{1}{2}\right)(1+v+(1-v)\cos(2\delta_i)),$$

$$U_V^K(x,s) = \sum_{m=0}^{\infty}[vs_0 f_K + vs_1 f'_K + vs_2 f''_K]\sin(m(\theta-\phi_i)) + [vc_0 f_K + vc_1 f'_K + vc_2 f''_K + vc_3 f'''_K]\cos(m(\theta-\phi_i)),$$

$$\Theta_V^K(x,s) = \sum_{m=0}^{\infty}[vs_0 g_K + vs_1 g'_K + vs_2 g''_K]\sin(m(\theta-\phi_i)) + [vc_0 g_K + vc_1 g'_K + vc_2 g''_K + vc_3 g'''_K]\cos(m(\theta-\phi_i)),$$

$k = 1,2,$

$$vc_0 = \left(\frac{m^2}{\rho_i^3}\right)(2\cos(\delta_i) + (1-v)\cos(2\delta_i)), \quad vs_0 = -\left(\frac{m^3}{\rho_i^3}\right)(1+(1-v)\cos(\delta_i))\sin(\delta_i).$$

$$vc_1 = \left(\frac{1}{\rho_i^2}\right)\left((1+m^2)\cos(\delta_i) + m^2(1-v)\cos(2\delta_i)\right), \quad vs_1 = \left(\frac{m}{\rho_i^2}\right)(1+\cos(\delta_i) - v\cos(\delta_i))\sin(\delta_i),$$

$$vc_2 = \frac{\cos(\delta_i)}{\rho_i}, \quad vs_2 = \left(\frac{m}{\rho_i}\right)(1+(v-1)\cos(\delta_i))\sin(\delta_i),$$

$$vc_3 = \cos(\delta_i).$$

## References


[1] H.B. Khurasia, S. Rawtani, Vibration analysis of circular plates with eccentric hole, *Journal of Applied Mechanics—Transactions of the ASME* 45 (1978) 215–217.

[2] A.W. Leissa, Y. Narita, Natural frequencies of simply supported circular plates, *Journal of Sound and Vibration* 70 (1980) 221–229.

[3] S.M. Vogel, D.W. Skinner, Natural frequencies of transversely vibrating uniform annular plates, *Journal of Applied Mechanics—Transactions o the ASME* 32 (1965) 926–931.

[4] D.A. Vega, S.A. Vera, M.D. Sanchez, P.A.A. Laura, Transverse vibrations of circular, annular plates with a free inner boundary, *Journal of the Acoustical Society of America* 103 (1998) 1225–1226.

[5] S.A. Vera, M.D. Sanchez, P.A.A. Laura, D.A. Vega, Transverse vibrations of circular, annular plates with several combinations of boundary conditions, *Journal of Sound and Vibration* 213 (4) (1998) 757–762.

[6] S.A. Vera, P.A.A. Laura, D.A. Vega, Transverse vibrations of a free–free circular annular plates, *Journal of Sound and Vibration* 224 (2) (1999) 379–383.

[7] J.T. Chen, S.Y. Lin, I.L. Chen, Y.T. Lee, Mathematical analysis and numerical study to free vibrations of annular plates using BIEM and BEM, *International Journal for Numerical Methods in Engineering* 65 (2006) 236–263.

[8] J.T. Chen, Y.T. Lee, I.L. Chen, K.H. Chen, Mathematical analysis and treatment for the true and spurious eigenequations of circular plates by the meshless method using radial basis function, *Journal of the Chinese Institute of Engineers* 27 (4) (2004) 547–561.
[9] K. Nagaya, K. Poltorak, Method for solving eigenvalue problems of the Helmholtz equation with a circular outer and a number of eccentric circular inner boundaries, *Journal of the Acoustical Society of America* 85 (1989) 576–581.
[10] K. Nagaya, T. Yamaguchi, Method for solving eigenvalue problems of the Helemholtz equation with an arbitrarily shaped outer and a number of eccentric circular inner boundaries, *Journal of the Acoustical Society of America* 90 (1991) 2146–2153.
[11] L. Cheng, Y.Y. Li, L.H. Yam, Vibration analysis of annular-like plates, *Journal of Sound and Vibration* 262 (2003) 1153–1170.
[12] P.A.A. Laura, U. Masia, D.R. Avalos, Small amplitude, transverse vibrations of circular plates elastically restrained against rotation with an eccentric circular perforation with a free edge, *Journal of Sound and Vibration* 292 (2006) 1004–1010.
[13] J.T. Chen, C.C. Hsiao, S.Y. Leu, Null-field integral equation approach for plate problems with circular holes, *Journal of Applied Mechanics—Transactions of the ASME* 73 (2006) 679–693.
[14] A.W. Leissa, Vibration of plates, NASA SP-160, 1969.
[15] C.P. Providatis, D.E. Beskos, Dynamic analysis of plates by boundary elements, *Applied Mechanics Reviews* 52 (7) (1999) 213–236.
[16] M. Tanaka, V. Sladek, J. Sladek, Regularization techniques applied to boundary element methods, *Applied Mechanics Reviews* 47 (1994) 457–499.
[17] J.T. Chen, H.K. Hong, Review of dual boundary element methods with emphasis on hypersingular integrals and divergent series, *Applied Mechanics Reviews—Transactions of the ASME* 52 (1) (1999) 17–33.
[18] J.T. Chen, W.C. Shen, P.Y. Chen, Analysis of circular torsion bar with circular holes using null-field approach, *Computer Modeling in Engineering Science* 12 (2) (2006) 109–119.
[19] J.T. Chen, W.C. Shen, A.C. Wu, Null-field integral equations for stress field around circular holes under anti-plane shear, *Engineering Analysis with Boundary Elements* 30 (2006) 205–217.
[20] E.S. Ventsel, An indirect boundary element method for plate bending analysis, *International Journal for Numerical Methods in Engineering* 40 (1997) 1597–1610.
[21] R. Kress, *Linear Integral Equations*, Springer, New York, 1989.
[22] R. Kress, On the numerical solution of a hypersingular integral equation in scattering theory, *Journal of Computational and Applied Mathematics* 61 (1995) 345–360.
[23] I.S. Gradshteyn, I.M. Ryzhik, *Table of Integrals, Series, and Products*, fifth ed., Academic Press, New York, 1996.
[24] M. Kitahara, *Boundary Integral Equation Methods in Eigenvalue Problems of Elastodynamics and Thin Plates*, Elsevier, Amsterdam, 1985.
[25] J.R. Hutchinson, Analysis of plates and shells by boundary collocation, in: D.E. Beskos (Ed.), *Boundary Elements Analysis of Plates and Shells*, Springer, Berlin, 1991, pp. 314–368.
[26] J.T. Chen, S.Y. Lin, I.L. Chen, Y.T. Lee, Mathematical analysis and numerical study to free vibrations of annular plates using BIEM and BEM, *International Journal for Numerical Methods in Engineering* 65 (2006) 236–263.
[27] M. Abramowitz, I.A. Stegun, *Handbook of Mathematical Functions*, Applied Mathematics Series National Bureau of Standards, Washington, DC, 1964.
[28] J.N. Reddy, *Mechanics of Laminated Composite Plates and Shells: Theory and Analysis*, CRC Press, Boca Raton, FL, 2004.
[29] C.S. Wu, Degenerate Scale Analysis for Membrane and Plate Problems Using the Meshless Method and Boundary Element Method, Master Thesis, National Taiwan Ocean University, Keelung, 2004.
[30] IMSL Math/Library Volumes 1 and 2, version 4.01 Visual Numerics, Inc., 1999.
[31] ABAQUS 6.5 Hibbitt, Karlsson and Sorensen, Inc., RI, 2004.